Nonlinearity **17** (2004) 2163–2186 PII: S0951-7715(04)68008-X

Rotating concentric circular peakons

Darryl D Holm[1,4], **Vakhtang Putkaradze**[2] **and Samuel N Stechmann**[1,3]

[1] Theoretical Division and Center for Nonlinear Studies, Los Alamos National Laboratory, MS B284, Los Alamos, NM 87545, USA
[2] Department of Mathematics and Statistics, University of New Mexico, Albuquerque, NM 87131-1141, USA
[3] Courant Institute of Mathematical Sciences, New York University, New York, NY 10025, USA

E-mail: dholm@lanl.gov, d.holm@imperial.ac.uk, putkarad@math.unm.edu, sam@t7.lanl.gov and stechman@cims.nyu.edu

Received 25 August 2003, in final form 5 July 2004
Published 16 August 2004
Online at stacks.iop.org/Non/17/2163
doi:10.1088/0951-7715/17/6/008

Recommended by E S Titi

Abstract

We study circularly symmetric solution behaviour of invariant manifolds of singular solutions of the partial differential equation EPDiff for geodesic flow of a pressureless fluid whose kinetic energy is the H^1 norm of the fluid velocity. These singular solutions describe interaction dynamics on lower-dimensional support sets, for example, curves, or filaments, of momentum in the plane. The 2 + 1 solutions we study are planar generalizations of the 1 + 1 peakon solutions of Camassa and Holm (1993 *Phys. Rev. Lett.* **71** 1661–4) for shallow water solitons. As an example, we study the canonical Hamiltonian interaction dynamics of N rotating concentric circles of peakons whose solution manifold is $2N$-dimensional. Thus, the problem is reduced from infinite dimensions to a finite-dimensional, canonical, invariant manifold. We show both analytical and numerical results. Just as occurs in soliton dynamics, these solutions are found to exhibit elastic collision behaviour. That is, their interactions exchange momentum and angular momentum but do not excite any internal degrees of freedom. One expects the same type of elastic collision behaviour to occur in other, more geometrically complicated cases.

PACS numbers: 47.35, 11.10.Ef, 45.20.Jj

(Some figures in this article are in colour only in the electronic version)

[4] Also at: Mathematics Department, Imperial College London, London SW7 2AZ, UK.

1. Introduction and overview

1.1. Geodesic flow by EPDiff in n dimensions

As first shown in Arnold [1], Euler's equations for ideal fluid dynamics represent geodesic motion on volume-preserving diffeomorphisms with respect to the the L^2 norm of the velocity. More generally, a time-dependent smooth map $g(t)$ is a geodesic on the diffeomorphisms with respect to a kinetic energy norm $\mathrm{KE} = \frac{1}{2}\|\boldsymbol{u}\|^2$, provided its velocity, the right-invariant tangent vector $\boldsymbol{u} = \dot{g}g^{-1}(t)$, satisfies the EPDiff equation [11, 12],

$$\frac{\partial}{\partial t}\boldsymbol{m} = -\boldsymbol{u}\cdot\nabla\boldsymbol{m} - \nabla\boldsymbol{u}^T\cdot\boldsymbol{m} - \boldsymbol{m}\,\mathrm{div}\,\boldsymbol{u} \equiv -\mathrm{ad}^*_{\boldsymbol{u}}\boldsymbol{m}. \tag{1}$$

EPDiff is short for *Euler–Poincaré equation on the diffeomorphisms*. Here ad* denotes the adjoint with respect to L^2 pairing, $\langle\cdot,\cdot\rangle : \mathfrak{g}^*\times\mathfrak{g}\to\mathbb{R}$, of the ad-action (commutator) of vector fields $\boldsymbol{u}, \boldsymbol{w} \in \mathfrak{g}$. That is,

$$\langle \mathrm{ad}^*_{\boldsymbol{u}}\boldsymbol{m}, \boldsymbol{w}\rangle = -\langle \boldsymbol{m}, \mathrm{ad}_{\boldsymbol{u}}\boldsymbol{w}\rangle = -\langle \boldsymbol{m}, [\boldsymbol{u}, \boldsymbol{w}]\rangle. \tag{2}$$

The momentum vector $\boldsymbol{m} \in \mathfrak{g}^*$ is defined as the variational derivative of kinetic energy with respect to velocity,

$$\delta(\mathrm{KE}) = \langle \boldsymbol{m}, \delta\boldsymbol{u}\rangle \iff \boldsymbol{m} = \frac{\delta(\mathrm{KE})}{\delta\boldsymbol{u}}. \tag{3}$$

This defining relation for momentum specifies the EPDiff equation (1) for geodesic motion in terms of the chosen kinetic energy metric $\mathrm{KE} = \frac{1}{2}\|\boldsymbol{u}\|^2$. For more details, extensions and applications of the Euler–Poincaré equation to both compressible and incompressible fluid and plasma dynamics, see Holm *et al* [12].

1.2. EPDiff flow with H^1 velocities in two dimensions

In this paper, we focus on the *solution behaviour* of the EPDiff equation (1) when its momentum vector is related to its velocity by the planar *two-dimensional* Helmholtz operation

$$\boldsymbol{m} = \boldsymbol{u} - \Delta\boldsymbol{u}, \tag{4}$$

where Δ denotes the Laplacian operator in the plane. This Helmholtz relation arises when the kinetic energy is given by the H^1 norm of the velocity,

$$\mathrm{KE} = \frac{1}{2}\|\boldsymbol{u}\|^2_{H^1} = \frac{1}{2}\int |\boldsymbol{u}|^2 + |\nabla\boldsymbol{u}|^2\,\mathrm{d}x\,\mathrm{d}y. \tag{5}$$

The H^1 kinetic energy norm (5) is an approximation of the Lagrangian in Hamilton's principle for columnar motion of shallow water over a flat bottom when the potential energy is negligible (the zero linear dispersion limit) and the kinetic energy of vertical motion is approximated by the second term in the integral [3]. In this approximation, the physical meaning of the quantity $\boldsymbol{m} = \delta(\mathrm{KE})/\delta\boldsymbol{u}$ in the Helmholtz relation (4) is the momentum of the shallow water flow, while $\boldsymbol{u}$ is its velocity in two dimensions. See Kruse *et al* [4] for details of the derivation of the geodesic EPDiff equation for approximating two-dimensional shallow water dynamics in this limit.

This paper determines the analytical and numerical properties of circularly symmetric solutions of the EPDiff equation (1) in the plane with definition (4). Remarkably, the solutions that emerge and dominate the circularly symmetric initial value problem for the EPDiff partial differential equation (1) are found to be *singular*. That is, their momenta are distributed on delta functions defined on rotating concentric circles in the plane, each of which moves with the velocity of the fluid at that radius. The corresponding velocity distribution has a peak located at each of these concentric circles, where it takes a jump in the radial derivative. Thus, the initial value problem for EPDiff with circular symmetry produces jumps in the derivative of the velocity moving with the flow when its kinetic energy is the H^1 norm. These are radially symmetric *contact discontinuities*. These emergent singular solutions are found to possess an invariant manifold governed by finite-dimensional canonical Hamiltonian dynamics. This dynamics exhibits elastic collision behaviour (with its associated momentum and angular momentum exchanges but no excitation of any internal degrees of freedom) just as occurs in soliton dynamics. One may expect the same type of elastic collision behaviour to occur in other, more geometrically complicated cases in the solution of the initial value problem for EPDiff.

1.3. Problem statement: geodesic flow with respect to H^1 in polar coordinates

The present work studies azimuthally symmetric solutions of the EPDiff equation (1) in polar coordinates (r, ϕ),

$$\boldsymbol{m} = m_r(r,t)\hat{\boldsymbol{r}} + m_\phi(r,t)\hat{\boldsymbol{\phi}} \qquad \text{and} \qquad \boldsymbol{u} = u_r(r,t)\hat{\boldsymbol{r}} + u_\phi(r,t)\hat{\boldsymbol{\phi}}, \tag{6}$$

in which the subscripts denote the radial and angular components. In the standard basis for polar coordinates, momentum one-forms and velocity vector fields are expressed as

$$\boldsymbol{m}\cdot \mathrm{d}\boldsymbol{x} = m_r\,\mathrm{d}r + rm_\phi\,\mathrm{d}\phi \qquad \text{and} \qquad \boldsymbol{u}\cdot\nabla = u_r\partial_r + \frac{u_\phi}{r}\partial_\phi. \tag{7}$$

Solutions (6) satisfy coupled partial differential equations whose radial and azimuthal components are, respectively,

$$\frac{\partial m_r}{\partial t} = -\frac{1}{r}\partial_r(rm_r u_r) - m_r\partial_r u_r - (rm_\phi)\partial_r\left(\frac{u_\phi}{r}\right), \tag{8}$$

$$\frac{\partial (rm_\phi)}{\partial t} = -\frac{1}{r}\partial_r(r^2 m_\phi u_r). \tag{9}$$

In these coupled equations, the nonzero rotation, u_ϕ, generates the radial velocity, u_r, which influences the azimuthal motion. Without rotation, $u_\phi = 0$ and $m_\phi = 0$; so the solution becomes purely radial. The system of equations (8) and (9) for geodesic motion conserves the H^1 kinetic energy norm,

$$\mathrm{KE}([u_r],[u_\phi]) = \frac{1}{2}\int\left[u_\phi^2 + u_{\phi,r}^2 + \frac{u_\phi^2}{r^2} + u_r^2 + u_{r,r}^2 + \frac{u_r^2}{r^2}\right] r\,\mathrm{d}r = \frac{1}{2}\|\boldsymbol{u}\|_{H^1}^2. \tag{10}$$

In the square brackets, the velocity components are denoted as in equation (6) and the subscript comma denotes the partial derivative. The corresponding momenta are defined by the dual relations

$$rm_\phi = \frac{\delta \mathrm{KE}}{\delta(u_\phi/r)} \qquad \text{and} \qquad m_r = \frac{\delta \mathrm{KE}}{\delta u_r}. \tag{11}$$

The Helmholtz relation (4), between m_ϕ and u_ϕ, for example, is expressed as

$$m_\phi = u_\phi - \frac{\partial^2 u_\phi}{\partial r^2} - \frac{1}{r}\frac{\partial u_\phi}{\partial r} + \frac{1}{r^2}u_\phi = \left(1 - \frac{1}{r}\partial_r r\partial_r + \frac{1}{r^2}\right)u_\phi. \tag{12}$$

This relation between velocity and momentum defines the Helmholtz operator in polar coordinates with finite boundary conditions at $r = 0$ and $\to \infty$. The velocity $u(r,t)$ is obtained from the momentum $m(r,t)$ by the convolution $u(r) = G * m = \int_0^\infty G(r,\xi)m(\xi)\xi\,\mathrm{d}\xi$ (an extra factor ξ arises in polar coordinates) with the Green function, $G(r, \xi)$. The Green function for the radial Helmholtz operator in (12) is given by

$$G(r, \xi) = \begin{cases} I_1(\xi)K_1(r) & \text{for } \xi < r, \\ I_1(r)K_1(\xi) & \text{for } r < \xi, \end{cases} \tag{13}$$

where I_1 and K_1 are modified Bessel's functions. This Green function will play a significant role in what follows.

Equations (8) and (9) may be written equivalently as a Hamiltonian system, by Legendre transforming the kinetic energy $\mathrm{KE}([u_r], [u_\phi])$ to the Hamiltonian $h([m_r], [rm_\phi])$, after which the equations take the form

$$\frac{\partial}{\partial t}\begin{bmatrix} m_r \\ rm_\phi \end{bmatrix} = \begin{bmatrix} \{m_r, h\} \\ \{rm_\phi, h\} \end{bmatrix} = -\mathcal{D}\begin{bmatrix} \delta h/\delta m_r \\ \delta h/\delta(rm_\phi) \end{bmatrix} = -\mathcal{D}\begin{bmatrix} u_r \\ u_\phi/r \end{bmatrix}, \tag{14}$$

where $\delta h/\delta m_r = u_r$, $\delta h/\delta(rm_\phi) = u_\phi/r$ and the Hamiltonian operator $\mathcal{D}$, is

$$\mathcal{D} = \begin{bmatrix} r^{-1}\partial_r r m_r + m_r\partial_r & rm_\phi\partial_r \\ r^{-1}\partial_r r^2 m_\phi & 0 \end{bmatrix}, \tag{15}$$

is the matrix $\mathcal{D} = \{(m_r, rm_\phi), (m_r, rm_\phi)\}$, which defines the Lie–Poisson bracket for geodesic motion in polar coordinates. As may be expected, $\mathcal{D}$ is skew-symmetric with respect to the L^2 pairing with radial measure $r\,\mathrm{d}r$.

2. Momentum maps and singular solutions of geodesic flow in n dimensions

2.1. Singular momentum solution ansatz for EPDiff

Based on the peakon solutions for the Camassa–Holm equation [2] and its generalizations to include the other travelling-wave pulson shapes [8], Holm and Staley [9] have introduced the following singular solution ansatz for the momentum of the EPDiff equation (1),

$$\boldsymbol{m}(\boldsymbol{x}, t) = \sum_{a=1}^{N}\int_s \boldsymbol{P}^a(s, t)\delta(\boldsymbol{x} - \boldsymbol{Q}^a(s, t))\,\mathrm{d}s, \qquad \boldsymbol{m} \in \mathbb{R}^n, \quad s \in \mathbb{R}^k, \tag{16}$$

where the dimensions satisfy $k < n$. These are singular momentum (weak) solutions, which are defined on subspaces of the ambient space. Being defined on delta functions, the singular solutions (16) have no internal degrees of freedom. They generalize the peakon solutions for the Camassa–Holm equation whose momenta are supported on points moving along the line. Having no internal degrees of freedom, these singular momentum solutions undergo elastic collisions as in soliton dynamics, without necessarily being integrable. (No claim is made here about the integrability of the singular solution dynamics.)

The fluid velocity corresponding to the singular momentum solution ansatz (16) is given by

$$\boldsymbol{u}(\boldsymbol{x}, t) = G * \boldsymbol{m} = \sum_{b=1}^{N}\int_{s'} \boldsymbol{P}^b(s', t)G(\boldsymbol{x}, \boldsymbol{Q}^b(s', t))\,\mathrm{d}s', \qquad \boldsymbol{u} \in \mathbb{R}^n, \tag{17}$$

where $G(\boldsymbol{x}, \boldsymbol{y})$ is the Green function for the Helmholtz operator in n dimensions. This velocity contains vector-valued momentum parameters $\boldsymbol{P}^b$ with $b = 1, \ldots, N$ that are supported in $\mathbb{R}^n$ on a set of N surfaces (or curves) of codimension $(n - k)$ for $s \in \mathbb{R}^k$ with $k < n$. In three dimensions, for example, these momentum parameters may be supported on sets of points (vector peakons, $k = 0$), quasi one-dimensional filaments (strings, $k = 1$), or quasi two-dimensional surfaces (sheets, $k = 2$). Substitution of the solution ansatz (16) into the

EPDiff equation (1) implies the following integro-partial-differential equations (IPDEs) for the evolution of such strings, or sheets,

$$\begin{aligned} \frac{\partial}{\partial t}\boldsymbol{Q}^a(s,t) &= \sum_{b=1}^{N}\int_{s'} \boldsymbol{P}^b(s',t)G(\boldsymbol{Q}^a(s,t),\boldsymbol{Q}^b(s',t))\,\mathrm{d}s', \\ \frac{\partial}{\partial t}\boldsymbol{P}^a(s,t) &= -\sum_{b=1}^{N}\int_{s'} (\boldsymbol{P}^a(s,t)\cdot\boldsymbol{P}^b(s',t))\frac{\partial}{\partial \boldsymbol{Q}^a(s,t)}G(\boldsymbol{Q}^a(s,t),\boldsymbol{Q}^b(s',t))\,\mathrm{d}s'. \end{aligned} \tag{18}$$

Importantly for the interpretation of these solutions given later in Holm and Marsden [11], the independent variables $s \in \mathbb{R}^k$ in the singular momentum ansatz (16) turn out to be Lagrangian coordinates. When evaluated along the curve $\boldsymbol{x} = \boldsymbol{Q}^a(s,t)$, the fluid velocity (17) satisfies [9]

$$\boldsymbol{u}(\boldsymbol{x},t)|_{\boldsymbol{x}=\boldsymbol{Q}^a(s,t)} = \sum_{b=1}^{N}\int_{s'} \boldsymbol{P}^b(s',t)G(\boldsymbol{Q}^a(s,t),\boldsymbol{Q}^b(s',t))\,\mathrm{d}s' = \frac{\partial \boldsymbol{Q}^a(s,t)}{\partial t}. \tag{19}$$

Consequently, the lower-dimensional support sets (defined on $\boldsymbol{x} = \boldsymbol{Q}^a(s,t)$ and parametrized by coordinates $s \in \mathbb{R}^k$) *move with the fluid velocity.*

Moreover, equations (18) for the evolution of these support sets are canonical Hamiltonian equations [9],

$$\frac{\partial}{\partial t}\boldsymbol{Q}^a(s,t) = \frac{\delta H_N}{\delta \boldsymbol{P}^a}, \qquad \frac{\partial}{\partial t}\boldsymbol{P}^a(s,t) = -\frac{\delta H_N}{\delta \boldsymbol{Q}^a}. \tag{20}$$

The corresponding Hamiltonian function, $H_N : (\mathbb{R}^n \times \mathbb{R}^n)^{\otimes N} \to \mathbb{R}$, is

$$H_N = \frac{1}{2}\int_s\int_{s'} \sum_{a,b=1}^{N} (\boldsymbol{P}^a(s,t)\cdot\boldsymbol{P}^b(s',t))G(\boldsymbol{Q}^a(s,t),\boldsymbol{Q}^b(s',t))\,\mathrm{d}s\,\mathrm{d}s'. \tag{21}$$

This is the Hamiltonian for canonical geodesic motion on the cotangent bundle of a set of N curves $\boldsymbol{Q}^a(s,t)$, $a = 1,\dots,N$, with respect to the metric given by G. The Hamiltonian (21) is obtained by substituting the weak solution ansatz (16) and (17) into $H = \frac{1}{2}\int \boldsymbol{m}\cdot\boldsymbol{u}\,\mathrm{d}^n x$.

The two- and three-dimensional solution behaviour arising from the weak solution ansatz (16) for the EPDiff equation (1) was investigated numerically in Holm and Staley [10]. We refer to that paper for the behaviour of the solution dynamics arising numerically from the initial value problem for equation (1) in the absence of circular symmetry and in higher dimensions.

Holm and Marsden [11] show that the singular momentum solution ansatz (16) is a momentum map. This fact explains why equations (20) are canonically Hamiltonian. It also explains why their corresponding Hamiltonian function (21) is obtained by substituting the solution ansatz (16) into the H^1 norm (5), which is the conserved energy for the EPDiff equation (1). All this is guaranteed by the momentum map property of the solution ansatz (16). However, this momentum map property does not explain why these singular solutions emerge and dominate the initial value problem for equation (1).

Aim of the paper. In this paper, we derive singular momentum solutions that are circularly symmetric in plane polar coordinates. For this circular symmetry, the nonlocality integrates out and the motion reduces to a dynamical system of *ordinary* differential equations. Most of the paper is devoted to the study of these circular solutions, which we call rotating peakons. The set of solutions obeying translational symmetry in the plane, but having two velocity components, is studied in appendix A. For a solution of N planar peakons, there are $2N$ degrees of freedom, with $2N$ positions and $2N$ canonically conjugate momenta. Hence, the evolution of the N planar peakon solution is governed by a set of $4N$ nonlocal partial differential equations. These reduce to ordinary differential equations in the presence of either rotational or translational symmetry. This paper also demonstrates numerically that these singular solutions emerge from any initial condition with this circular symmetry in the plane. Thus, the singular solutions (16) are an essential feature of the initial value problem for equation (1). In appendix B, we generalize the circularly symmetric singular solutions in two dimensions to cylindrically symmetric singular solutions, with axial translation symmetry in three dimensions.

2.2. Potential applications of singular EPDiff solutions

One of the potential applications of the two-dimensional version of this problem involves the internal waves on the interface between two layers of different density in the ocean. Figure 1 shows a striking agreement between two internal wave trains propagating at the interface of different density levels in the South China Sea, and the solution appearing in the simulations of the EPDiff equation (1) in two dimensions. Inspired by this figure, we shall construct a theory of propagating one-dimensional momentum filaments in two dimensions. For other work on the two-dimensional CH equation in the context of shallow water waves, see Kruse *et al* [4].

Another potential application of the two-dimensional version of this problem occurs in image processing for computational anatomy, e.g. brain mapping from PET scans. For this application, one envisions the geodesic motion as an optimization problem whose solution maps one measured two-dimensional PET scan to another by interpolation in three dimensions along a geodesic path between them in the space of diffeomorphisms. In this situation, the singular solutions of geodesic flow studied here correspond to 'cartoon' outlines of PET scan images. The geodesic 'evolution' in the space between them provides a three-dimensional image that is optimal for the chosen norm. For a review of this imaging approach, which is called 'template matching' in computational anatomy, see Miller and Younes [13]. For recent discussions of the relation of soliton dynamics to computational anatomy in the context of EPDiff, see Holm *et al* [14].

2.3. Peakon momentum map $J : T^*S \longrightarrow \mathfrak{g}^*$ in n dimensions

Holm and Marsden [11] have explained an important component of the general theory underlying the remarkable reduced solutions of the vector EPDiff equation (1). In particular, Holm and Marsden [11] have shown that the solution ansatz (16) for the momentum vector in the EPDiff equation (1) introduced in Holm and Staley [9] defines a momentum map for the (left) action of diffeomorphisms on the support sets $\mathcal{S}$ of the Dirac delta functions. These support sets are points on the real line for the CH shallow water equation in one dimension. They are points, curves, or surfaces in $\mathbb{R}^n$ for the vector EPDiff equation (1) in n dimensions.

Momentum map definition. Let a group G act on a manifold S and lift the action of G to the cotangent bundle T^*S. This lifted action yields a Poisson map J from T^*S to $\mathfrak{g}^*$, the dual of the Lie algebra of G. (A map is Poisson, provided it is coadjoint equivariant. In particular, J maps the canonical Poisson bracket on the image space T^*S into the Lie–Poisson bracket on the target space $\mathfrak{g}^*$.) In symbols, this is

$$J : (\boldsymbol{P}, \boldsymbol{Q}) \in T^*S \longrightarrow \boldsymbol{m} \in \mathfrak{g}^*,$$

$$J : \{f, h\}_{\mathrm{can}}(\boldsymbol{P}, \boldsymbol{Q}) \longrightarrow \{f, h\}_{\mathrm{LP}}(\boldsymbol{m}) = \left\langle \boldsymbol{m}, \left[\frac{\delta f}{\delta \boldsymbol{m}}, \frac{\delta h}{\delta \boldsymbol{m}}\right]\right\rangle, \qquad \text{where } \langle\cdot,\cdot\rangle : \mathfrak{g}^* \times \mathfrak{g} \longrightarrow \mathbb{R}.$$

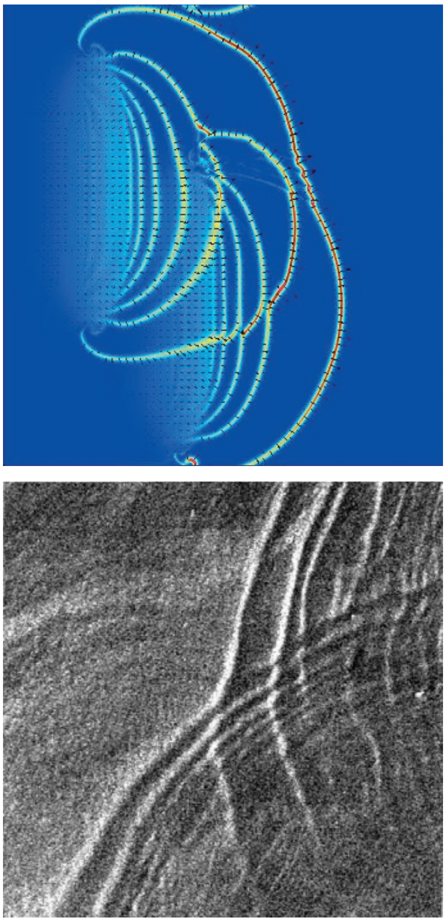

Figure 1. Simulation of the full EPDiff equation (1), courtesy of Martin Staley (top). Internal waves in the South China Sea (bottom).

A Poisson map $J : T^*S \to \mathfrak{g}^*$ that satisfies

$$\langle J(\alpha_q), \xi\rangle = \langle \alpha_q, \xi_Q(q)\rangle \tag{22}$$

for any $\alpha_q \in T^*S$ and $\xi \in \mathfrak{g}$ is called a momentum map. For details of the many properties and rich mathematical features of momentum maps, see Ortega and Ratiu [15]. The approach we use to characterize equivariant momentum maps is explained in an interesting way in section 3 of Weinstein [16].

The n-dimensional peakon momentum solution ansatz (for any Hamiltonian) introduced by Holm and Staley [9] is the superposition formula in equation (16), which is now regarded as a map $J : T^*S \to \mathfrak{g}^*$, given by

$$J : \boldsymbol{m}(\boldsymbol{x}, t) = \sum_{a=1}^{N} \int_s \boldsymbol{P}^a(s,t)\delta(\boldsymbol{x} - \boldsymbol{Q}^a(s,t))\,\mathrm{d}s, \qquad \boldsymbol{m} \in \mathbb{R}^n, \quad s \in \mathbb{R}^k. \tag{23}$$

By direct substitution using the canonical $\boldsymbol{Q}, \boldsymbol{P}$ Poisson brackets, one computes the *Poisson property* of the map J in n Cartesian dimensions. Namely,

$$\{m_i(\boldsymbol{x}), m_j(\boldsymbol{y})\}_{\mathrm{can}}(\boldsymbol{P}, \boldsymbol{Q}) = -\left(\frac{\partial}{\partial x^j}\, m_i(\boldsymbol{x}) + m_j(\boldsymbol{x})\frac{\partial}{\partial x^i}\right)\delta(\boldsymbol{x} - \boldsymbol{y}) \tag{24}$$

in the sense of distributions integrated against a pair of smooth functions of $\boldsymbol{x}$ and $\boldsymbol{y}$. This expression defines the Lie–Poisson bracket $\{\cdot,\cdot\}_{\mathrm{LP}}(\boldsymbol{m})$ defined on the dual Lie algebra $\mathfrak{g}^*$, restricted to momentum filaments supported on the N curves $\boldsymbol{x} = \boldsymbol{Q}^a(s,t)$, where $a = 1, 2, \ldots, N$. The singular momentum ansatz J in the map (23) was verified to satisfy the defining relation for momentum maps (22) in Holm and Marsden [11]. Hence the following theorem.

Theorem 2.1 (Holm and Marsden [11]). *The momentum solution ansatz (16) for singular solutions of the vector EPDiff equation (1) is a momentum map.*

The momentum map J in (16), (23) is, of course, independent of the choice of Hamiltonian. This independence explains, for example, why the map extends from peakons of a particular shape in Camassa and Holm [2] to the pulsons of any shape studied in Fringer and Holm [8]. The solution ansatz (16), now rewritten as the momentum map J in (23), is also a Lagrange-to-Euler map because the momentum is supported on filaments that *move with the fluid velocity*. Hence, the motion governed by the EPDiff equation (1) occurs by the action of the diffeomorphisms in G on the support set of the fluid momentum, whose position and *canonical* momentum are defined on the cotangent bundle T^*S of the space of curves S. This observation informs the study of geodesic motion governed by the EPDiff equation (1). For complete details and definitions, we refer to Holm and Marsden [11].

2.4. Peakon momentum map $J : T^*S \longrightarrow \mathfrak{g}^*$ on a Riemannian manifold

The goal of the present work is to characterize the singular momentum solutions of the vector EPDiff equation (1) by using the momentum map J in (23) when S is the space of concentric circles in the plane. The motion and interactions of these singular momentum solutions may be purely radial (circles of peakons), or they may also have an azimuthal component (rotating circles of peakons). To accomplish this goal, we employ a result from Holm and Staley [10] that on a Riemannian manifold M with metric determinant $\det g(\boldsymbol{x})$, the singular momentum ansatz (16) becomes

$$\boldsymbol{m}(\boldsymbol{x},t) = \sum_{a=1}^{N} \int_s \boldsymbol{P}^a(s,t) \frac{\delta(\boldsymbol{x} - \boldsymbol{Q}^a(s,t))}{\sqrt{\det g}}\, \mathrm{d}s, \qquad \boldsymbol{m} \in M, \quad s \in \mathbb{R}^k. \tag{25}$$

This solution ansatz is also a momentum map, as shown in Holm and Marsden [11]. On a Riemannian manifold, the corresponding Lie–Poisson bracket for the momentum on its support set becomes

$$\{m_i(\boldsymbol{x}), m_j(\boldsymbol{y})\} = -\left(m_j(\boldsymbol{x}) \frac{\partial}{\partial x^i} + \frac{1}{\sqrt{\det g}} \frac{\partial}{\partial x^j} \sqrt{\det g}\, m_i(\boldsymbol{x}) \right) \frac{\delta(\boldsymbol{x} - \boldsymbol{y})}{\sqrt{\det g}}. \tag{26}$$

For example, in polar coordinates one has $\sqrt{\det g} = r$ and the vector $\boldsymbol{m}$ depends only on the radial coordinate, r. For solutions with these symmetries, the Lagrangian label coordinate, s, is unnecessary, as we shall see in polar coordinates, and the equations for $\boldsymbol{Q}^a$ and $\boldsymbol{P}^a$ will reduce to ordinary differential equations in time. Equation (26) for the singular Lie–Poisson bracket on a Riemannian manifold is a new result.

3. Lie–Poisson bracket for rotating concentric circles of peakons

3.1. Azimuthal relabelling symmetry for rotating circular peakons

We shall consider the dynamics of rotating circular peakons, whose motion may have both radial and azimuthal components. Suppose one were to mark a Lagrangian point on the ath circle, $a = 1, \ldots, N$. Then the change in its azimuthal angle, $\phi_a(t)$, could be measured as it moves with the azimuthal fluid velocity, u_ϕ, along the the ath circle as its radius $r = q_a(t)$ evolves. Translations in the Lagrangian azimuthal coordinate would shift the mark, but this shift of a Lagrangian label would have no effect on the Eulerian velocity dynamics of the system. Such a Lagrangian relabelling would be a symmetry for any Hamiltonian, depending only on the Eulerian velocity. Thus, the azimuthal relabelling would result in the conservation of its canonically conjugate angular momentum, M_a, which generates the rotation corresponding to the relabelling symmetry of the ath circle. The ath circle would be characterized in phase space by its radius, $r = q_a(t)$, and its canonically conjugate radial momentum, denoted as p_a. The rotational degree of freedom of the ath circle would be represented by its conserved angular momentum, M_a, and its ignorable canonical azimuthal angle, ϕ_a. The only nonzero canonical Poisson brackets among these variables are

$$\{q_a, p_b\}_{\mathrm{can}} = \delta_{\mathrm{ab}} \qquad \text{and} \qquad \{\phi_a, M_b\}_{\mathrm{can}} = \delta_{\mathrm{ab}}. \tag{27}$$

3.2. *Poisson map for rotating circular peakons*

In terms of their $4N$ canonical phase space variables (q_a, p_a, ϕ_a, M_a), with $a = 1, 2, \ldots, N$, the superposition formula (23) for N rotating circular peakons may be expressed as

$$\mathcal{J} : \boldsymbol{m}(r,t) = \sum_{a=1}^{N} \left(p_a(t)\hat{\boldsymbol{r}} + \frac{M_a}{q_a(t)}\hat{\phi} \right) \frac{\delta(r - q_a(t))}{r}. \tag{28}$$

We shall verify that this formula is a Poisson map, and then in section 4 we shall rederive it, by requiring it to be a valid solution ansatz for the EPDiff equation (1) in polar coordinates. In fact, formula (28) is more than just a Poisson map. It is also the special case for plane polar coordinates of the momentum map discussed in Holm and Marsden [11]. As a consequence, the motion governed by the system of partial differential equations (8) and (9) for planar EPDiff with azimuthal symmetry has a finite-dimensional invariant manifold in the $2N$-dimensional canonical phase space (q_a, p_a) for each choice of the N angular momentum values M_a, with $a = 1, 2, \ldots, N$. Later, we shall also examine numerical studies of these solutions when the kinetic energy is chosen to be the H^1 norm of the azimuthally symmetric fluid velocity.

By direct substitution using the canonical Poisson brackets in (27), one verifies the Poisson property of the map $\mathcal{J}$ in (28) as follows,

$$\begin{aligned}
\{m_r(r), m_r(r')\}_{\mathrm{can}}(\boldsymbol{p}, \boldsymbol{q}) &= -\left(\frac{1}{r}\frac{\partial}{\partial r} r m_r(r) + m_r(r)\frac{\partial}{\partial r} \right) \frac{\delta(r - r')}{r}, \\
\{m_r(r), r' m_\phi(r')\}_{\mathrm{can}}(\boldsymbol{p}, \boldsymbol{q}) &= -r m_\phi(r)\frac{\partial}{\partial r}\frac{\delta(r - r')}{r}, \\
\{r m_\phi(r), m_r(r')\}_{\mathrm{can}}(\boldsymbol{p}, \boldsymbol{q}) &= -\frac{1}{r}\frac{\partial}{\partial r} r^2 m_\phi(r)\frac{\delta(r - r')}{r}, \\
\{r m_\phi(r), r m_\phi(r')\}_{\mathrm{can}}(\boldsymbol{p}, \boldsymbol{q}) &= 0.
\end{aligned} \tag{29}$$

These equalities are written in the sense of distributions integrated against a pair of smooth functions of r and r'. They demonstrate the Poisson property of the map $\mathcal{J}$ in (28), which is also the solution ansatz for the rotating circular peakons. They also express the Lie–Poisson bracket $\{\cdot, \cdot\}_{\mathrm{LP}}(m_r, r m_\phi)$ for momentum filaments defined on the dual Lie algebra $\mathfrak{g}^*$ and restricted to the support set of these solutions. Hence, we have demonstrated the following proposition.

Proposition 3.1. *The map $\mathcal{J}$ in (28) is a Poisson map.*

On comparing the formulae in (29) with the Hamiltonian operator $\mathcal{D}$ for the continuous solutions in (15), one sees that the momentum map (28) restricts the Lie–Poisson bracket with Hamiltonian operator $\mathcal{D}$ to its support set. Next, we shall rederive the Poisson map (28) by requiring it to be a valid solution ansatz for the geodesic EPDiff equation (1) in polar coordinates.

4. Azimuthally symmetric peakons

4.1. Derivation of equations

We seek azimuthally symmetric solutions of the geodesic EPDiff equation (1) in polar coordinates (r, ϕ), for which

$$\boldsymbol{m} = m_r(r,t)\hat{\boldsymbol{r}} + m_\phi(r,t)\hat{\boldsymbol{\phi}} \equiv (m_r(r,t), m_\phi(r,t)). \tag{30}$$

We shall rederive the momentum map (28) and the canonical Hamiltonian equations for its parameters (q_a, p_a, M_a) by assuming solutions in the form

$$\boldsymbol{m}(r,t) = \sum_{i=1}^{N} (p_i(t)\hat{\boldsymbol{r}} + v_i(t)\hat{\boldsymbol{\phi}}) \frac{\delta(r - q_i(t))}{r}. \tag{31}$$

These solutions represent concentric circular momentum filaments that are rotating around the origin. The corresponding velocity components are obtained from

$$(u_r(r,t), u_\phi(r,t)) = \int r' G(r,r')(m_r(r',t), m_\phi(r',t))\,\mathrm{d}r', \tag{32}$$

where $G(r,r') = G(r',r)$ is the (symmetric) Green function for the radial Helmholtz operator given in formula (13). Hence, the fluid velocity corresponding to the solution ansatz (31) assumes the form

$$\boldsymbol{u}(r,t) = \sum_{j=1}^{N} (p_j(t)\hat{\boldsymbol{r}} + v_j(t)\hat{\boldsymbol{\phi}}) G(r, q_j(t)), \tag{33}$$

with Green function, $G(r, q_j(t))$, as in formula (13). In addition, the kinetic energy of the system is given by

$$\mathrm{KE}(\boldsymbol{p}, \boldsymbol{q}, \boldsymbol{v}) = \frac{1}{2}\int \boldsymbol{u}\cdot\boldsymbol{m} r\,\mathrm{d}r = \frac{1}{2}\sum_{i,j=1}^{N} (p_i p_j + v_i v_j) G(q_i, q_j). \tag{34}$$

Substitution of the solution ansatz (31) for the momentum and its corresponding velocity (33) into the radial equation (8) gives the system

$$\begin{aligned}
\sum_i \left(\dot{p}_i \frac{\delta(r-q_i)}{r} - p_i \dot{q}_i \frac{\delta'(r-q_i)}{r} \right) + \sum_{i,j} \Bigg\{ & p_i p_j G(r,q_j) \left[-\frac{\delta(r-q_i)}{r^2} + \frac{\delta'(r-q_i)}{r} \right] \\
& + 2 p_i p_j \frac{\delta(r-q_i)}{r} \frac{\partial G}{\partial r}(r,q_j) + (p_i p_j - v_i v_j) \frac{\delta(r-q_i)}{r^2} G(r,q_j) \\
& + v_i v_j \frac{\delta(r-q_i)}{r} \frac{\partial G}{\partial r}(r,q_j) \Bigg\} = 0.
\end{aligned}$$

Multiplying this system by the smooth test function $r\psi(r)$ and integrating with respect to r yields dynamical equations for p_i and q_i. In particular, the $\psi(q_i)$ terms yield

$$\dot{p}_i = -\sum_j \left(p_i p_j \frac{\partial G}{\partial q_i} + v_i v_j \left\{ \frac{\partial G(q_i,q_j)}{\partial q_i} - \frac{G(q_i,q_j)}{q_i} \right\} \right) \tag{35}$$

and after integrating by parts, the $\psi'(q_i)$ terms yield

$$\dot{q}_i = \sum_j p_j G(q_i, q_j). \tag{36}$$

By equation (33) we see that $\dot{q}_i(t) = \hat{\boldsymbol{r}} \cdot \boldsymbol{u}(q_i, t)$, so the radius of the ith cylinder moves with the radial velocity of the flow.

This procedure is repeated for the ϕ component of the EPDiff equation by substituting the solution ansatz (31) and (33) into equation (9), to find the system

$$\sum_i \left(\dot{v}_i \frac{\delta(r - q_i)}{r} - v_i \dot{q}_i \frac{\delta'(r - q_i)}{r} \right) + \sum_{i,j} \left\{ v_i p_j G(r, q_j) \left[-\frac{\delta(r - q_i)}{r^2} + \frac{\delta'(r - q_i)}{r} \right] \right.$$
$$\left. + v_i p_j \frac{\delta(r - q_i)}{r} \left(\frac{\partial G}{\partial r}(r, q_j) + 2\frac{G(r, q_j)}{r} \right) \right\} = 0.$$

Upon multiplying this system by $r\psi(r)$ and integrating with respect to r, the term proportional to $\psi'(q_i)$ again recovers exactly the q_i equation (36). The term proportional to $\psi(q_i)$ gives

$$\dot{v}_i = -\frac{v_i}{q_i} \sum_j p_j G(q_i, q_j) = -v_i \frac{\dot{q}_i}{q_i} \tag{37}$$

after using the q_i equation (36) in the last step. This integrates to

$$v_i q_i = M_i = \text{const}, \tag{38}$$

where M_i are N integration constants. From the Hamiltonian viewpoint, this was expected: the angular momentum, M_i, is conserved for each circular peakon because each circle may be rotated independently without changing the energy.

Equations (35) and (36) for p_i and q_i may now be recognized as Hamilton's canonical equations with Hamiltonian

$$H(\boldsymbol{p}, \boldsymbol{q}, \boldsymbol{M}) = \frac{1}{2}\int \boldsymbol{u} \cdot \boldsymbol{m} r \, \mathrm{d}r = \frac{1}{2} \sum_{i,j=1}^{N} \left(p_i p_j + \frac{M_i M_j}{q_i q_j} \right) G(q_i, q_j). \tag{39}$$

This is the same Hamiltonian as obtained from substituting the momentum map (28) into the kinetic energy, KE, in equation (34). Hence, we may recover the reduced equations (35) for p_i, equation (36) for q_i and equation (38) for M_i from the Hamiltonian (39) and the canonical equations,

$$\dot{p}_i = -\frac{\partial H}{\partial q_i}, \qquad \dot{q}_i = \frac{\partial H}{\partial p_i}, \qquad \dot{M}_i = -\frac{\partial H}{\partial \phi_i} = 0. \tag{40}$$

This result proves the following proposition.

Proposition 4.1. *The Poisson map (28) is a valid ansatz for rotating peakon solutions of the EPDiff equation (1) for geodesic motion.*

This is the explicit result for plane polar coordinates of the general theorem presented in Holm and Marsden [11] for the singular momentum map arising from the left action of diffeomorphisms on smoothly embedded subspaces in $\mathbb{R}^n$. The dynamics reduces to canonical Hamiltonian equations (40) precisely because the Poisson map (28) is a momentum map.

4.2. Solution properties

The remaining canonical equation for the ith Lagrangian angular frequency is,

$$\dot{\phi}_i = \frac{\partial H}{\partial M_i} = \sum_j \frac{M_j}{q_i q_j} G(q_i, q_j) = \frac{1}{q_i} \sum_j v_j(t) G(q_i, q_j). \tag{41}$$

Thus, as expected, the ignorable canonical angle variables $\phi = \{\phi_i\}$, with $i = 1, 2, \ldots, N$, decouple from the other Hamiltonian equations. In addition, we see that

$$q_i \dot{\phi}_i(t) = \hat{\phi} \cdot \boldsymbol{u}(q_i, t) \tag{42}$$

and so the angular velocity of the ith cylinder *also* matches the angular velocity of the flow. Therefore, we have shown the following proposition.

Proposition 4.2. *The canonical Hamiltonian parameters in the momentum map and solution ansatz (28) provide a Lagrangian description in polar coordinates of the flow governed by the EPDiff equation (1).*

Angular momentum, fluid circulation, and collapse to the centre. Finally, the fluid circulation of the ith concentric circle, c_i, which is travelling with velocity $\boldsymbol{u}$, may be computed from equations (30) and (31) (with a slight abuse of notation) as

$$\oint_{c_i(\boldsymbol{u})} \boldsymbol{m} \cdot \mathrm{d}\boldsymbol{x} = \oint_{c_i(\boldsymbol{u})} r m_\phi \mathrm{d}\phi = 2\pi v_i = \frac{2\pi M_i}{q_i}. \tag{43}$$

We see that the 'angular velocity' $v_i = M_i/q_i$ is the fluid circulation of the ith concentric circle. Since the angular momentum, M_i, of the ith circle is conserved, its circulation, $v_i(t)$, varies inversely with its radius. Consequently, this circulation would diverge if the ith circle were to collapse to the centre with nonzero angular momentum.

Remark. As mentioned earlier, propositions 3.1, 4.1, and 4.2 are special cases for circular symmetry of a general theorem for the singular momentum map presented in Holm and Marsden [11].

5. Numerical results for radial peakons

5.1. Radial peakon collisions

We consider purely radial solutions of equation (8), with $m_\phi = 0$, that satisfy

$$\frac{\partial m_r}{\partial t} = -\frac{1}{r}\partial_r(r m_r u_r) - m_r \partial_r u_r. \tag{44}$$

Such radial solutions have no azimuthal velocity. Without azimuthal velocity, the vector peakon solution ansatz (31) for momentum reduces to the scalar relation

$$m_r(r, t) = \sum_{i=1}^{N} p_i(t) \frac{\delta(r - q_i(t))}{r}. \tag{45}$$

The corresponding radial velocity is

$$u_r(r, t) = \sum_{i=1}^{N} p_i(t) G(r, q_i(t)), \tag{46}$$

where the Green function, $G(r, q_i(t))$, for the radial Helmholtz operator is given by formula (13). Radial peakons of this form turn out to be the building blocks for the solution of

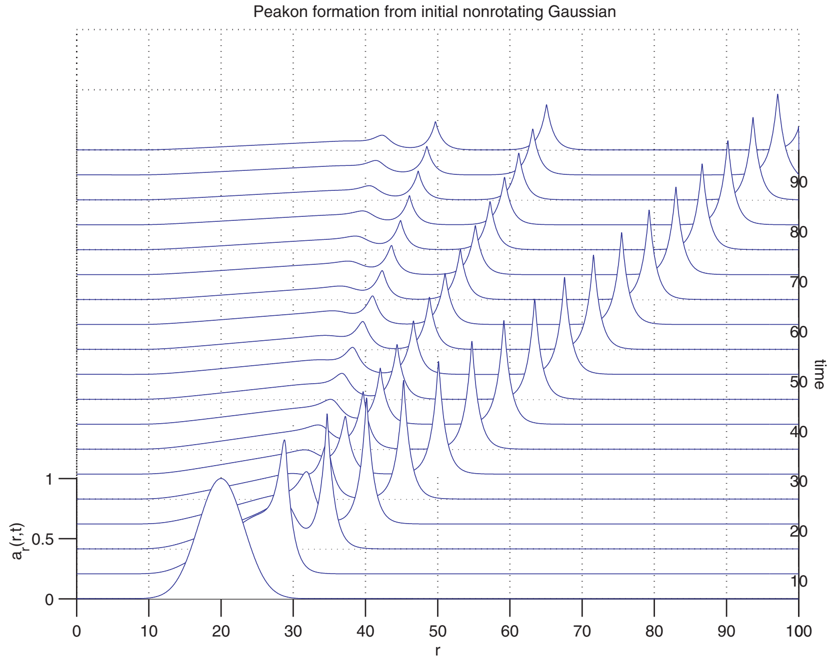

Figure 2. The initial value problem: a Gaussian profile splits into peakons.

any radially symmetric initial value problem. We have found numerically that the initial value problem for equation (45) with any initially confined radial distribution of velocity quickly splits up into radial peakons. This behaviour is illustrated in figure 2. The initial distribution of velocity splits almost immediately into a train of radial peakons arranged by height or, equivalently, speed.

The head-on 'peakon–antipeakon' collisions are of special interest. In the case of equal strength radial peakon–antipeakon collisions, the solution appears to develop an infinite slope in finite time, see figure 3. This behaviour is also known to occur for peakon–antipeakon collisions on the real line. If the strengths of the peakon and antipeakon are not equal, then the larger one of them seems to 'plough' right through the smaller one. This is shown in figure 4.

The figures shown were produced from numerical simulations of the Eulerian PDE (44). The momentum, m_r, was advanced in time using a fourth-order Runge–Kutta method. The time step was chosen to ensure the Hamiltonian $\frac{1}{2}\int \boldsymbol{m}\cdot\boldsymbol{u}r\,\mathrm{d}r$ was conserved to within 0.1% of its initial value. The spatial discretizations ranged from $\mathrm{d}r = 10^{-4}$ to $\mathrm{d}r = 0.02$, depending on the desired resolution and the length of the spatial domain, and the spatial derivatives were calculated using finite differences. Fourth- and fifth-order centred differencing schemes were used for the first and second derivatives, respectively. The momentum, m_r, was found from the velocity, u_r, using the finite difference form of the radial Helmholtz operator, and the velocity, u_r, was found from the momentum, m_r, by inverting the radial Helmholtz matrix. For the peakon interaction simulations, the initial conditions were given by a sum of peakons of the form (46) for some chosen initial p_i and q_i. For a peakon collapsing to the centre, which will be described next, the boundary condition at the origin is important. If the PDE (44) were extended to $r < 0$, then the velocity would be an *odd* function about the origin. In addition, when the peakon was sufficiently close to the origin ($q_i < 0.1$), the sign of its momentum m_r was reversed to begin its expansion away from the origin.

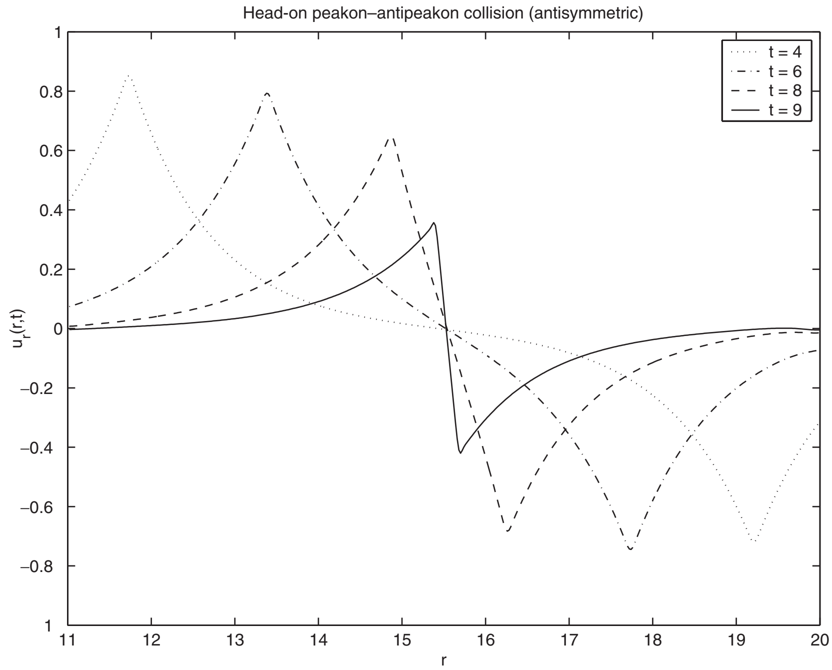

Figure 3. Peakon–antipeakon collision of equal strength.

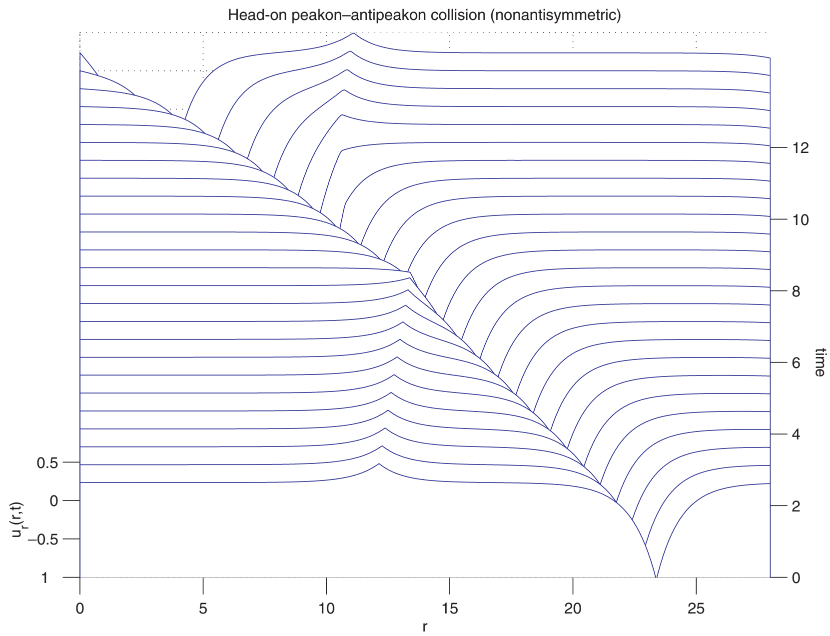

Figure 4. Peakon–antipeakon collision of unequal strength. The smaller peakon's trajectory undergoes a large phase shift.

For comparison with the simulations of the Eulerian PDE (44), simulations of the Lagrangian ODEs (40) were also performed. A fourth-order Runge–Kutta method was used to advance the system in time, and a time step was chosen to ensure the Hamiltonian (39) was conserved to within 0.1%. The results of these simulations agreed with those of the Eulerian PDE simulations to within 1%.

5.2. Bouncing off the centre

Let us first consider the case when only one peakon collapses onto the centre with the angular momentum being zero. The Hamiltonian in this case is

$$H = \tfrac{1}{2} p^2 I_1(q) K_1(q),$$

which can be approximated when $q \to 0$ as

$$H = \left(\tfrac{1}{4} + o(q)\right) p^2.$$

Thus, the momentum $p(t)$ is nearly constant just before the collapse time, t_*, and is approximately equal to $-2\sqrt{H}$; more precisely,

$$p = -2\sqrt{H} + o(q).$$

The equation of motion for $q(t)$ yields $\dot{q} = pI_1(q)K_1(q) = -\sqrt{H} + o(q)$. If $q \to 0$ at $t \to t_*$, then we necessarily have

$$q(t) = \sqrt{H}(t_* - t) + o((t_* - t)^2)$$

near the time of collapse $t \to t_*$.

The case of N radial peakons can be considered similarly. If only one peakon (let us say, number a) collapses into the centre at time t_*, so that $q_a(t) \to 0$ as $t \to t_*$, and the motion of the peakons away from the centre is regular in some interval $(t_* - \delta, t_* + \delta)$ (as will be the case unless a peakon–antipeakon collision occurs during this interval), then conservation of the Hamiltonian implies

$$p_a^2 G(q_a, q_a) + 2p_a A + B = 2H, \tag{47}$$

where

$$A = \sum_{i \neq a} p_i G(q_a, q_i),$$

$$B = \sum_{(i,j) \neq a} p_i p_j G(q_i, q_j).$$

Since $q_a = \min(q_1, \ldots, q_N)$, the Helmholtz Green function in expression (13) implies that the quantities A and B are bounded at times close to t_* and that $G(q_a, q_a)$ is bounded as well. Consequently, equation (47) implies that p_a is also bounded at times close to $t = t_*$.

Numerical simulations confirm our predictions: at the moment of the impact at the centre, the amplitude of the peakon remains bounded and approaches the value of $-\sqrt{H} \approx -2.23$, as illustrated in figure 5.

The slope of the solution at the origin has to diverge. This can be seen on the example of a single peakon as follows. Since

$$\left.\frac{\partial u}{\partial r}\right|_{r=0} = p(t) I_1'(0) K_1(q) = \frac{1 + o(q)}{2} \frac{p(t)}{q(t)},$$

if $q(t) \to 0$ as $t \to t_*$, the slope $\partial_r u(r = 0, t)$ must diverge. Therefore, the following proposition is true.

Proposition 5.1. *A radially symmetric peakon with no angular momentum, collapsing to the centre, has bounded momentum and unbounded slope at the origin close to the moment of collapse.*

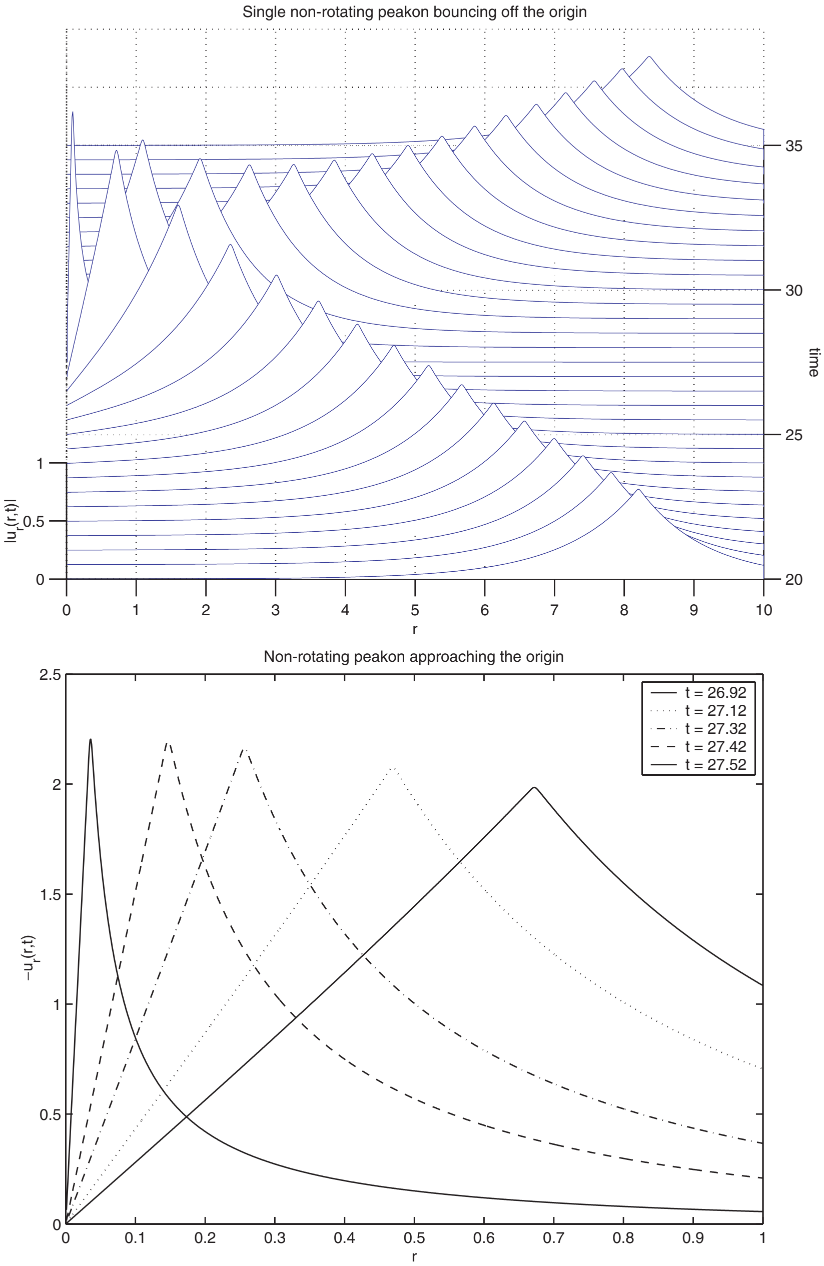

Figure 5. Impact of a peakon onto the centre.

6. Numerical results for rotating peakon circles

Simulations of rotating peakons were performed for the Eulerian system of PDEs (8) and (9) using the same numerical methods as those used for nonrotating peakons. Figure 6 shows the results of an initial value problem simulation when u_r is initially 0 and u_ϕ is initially a Gaussian function. A radial velocity in both directions is almost immediately generated, and

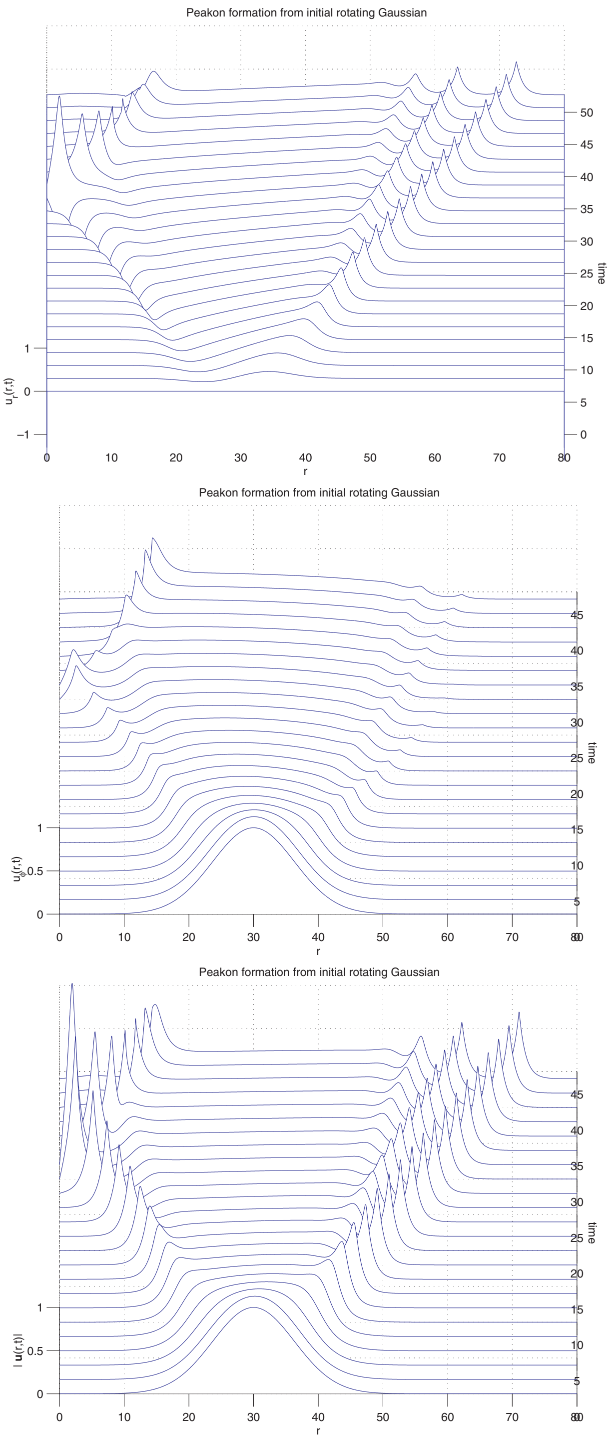

Figure 6. An initial angular velocity distribution (with zero initial radial velocity) breaks up into rotating peakons that move both inwards and outwards. The radial velocity, u_r, the angular velocity, u_ϕ, and the velocity magnitude, $|\boldsymbol{u}|$, are all shown.

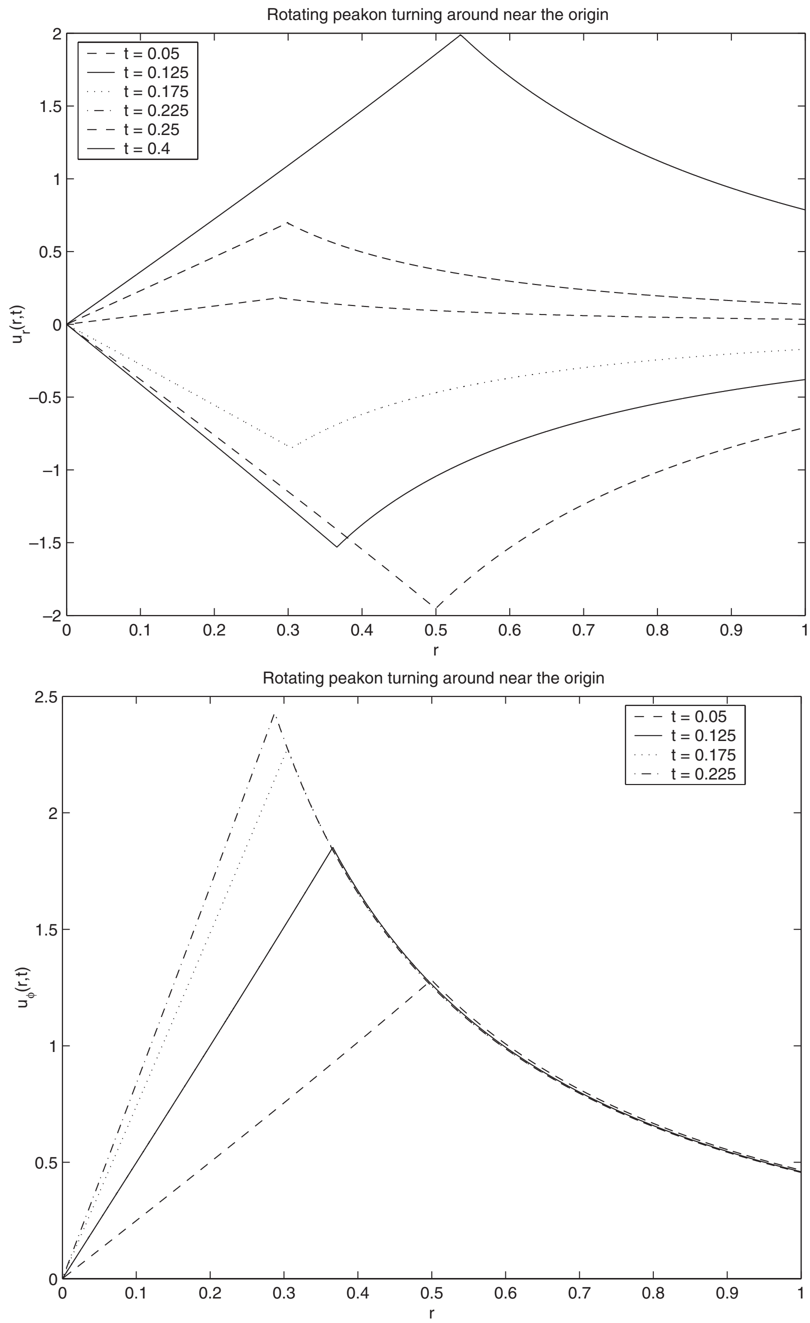

Figure 7. A rotating peakon turns around near the origin. The radial velocity changes sign as the angular velocity reaches a maximum.

rotating peakons soon emerge, moving both inwards and outwards but all rotating in the same direction. A rotating peakon approaches the centre but turns around before reaching the origin.

Figure 7 shows a rotating peakon as it approaches the origin. A sort of angular momentum barrier is reached, and the peakon turns around and moves away from the origin. Thus, a peakon's behaviour as it approaches the origin is reminiscent of Sundman's theorem. Sundman's theorem states that three or more bodies with nonzero total angular momentum will not all simultaneously collide. Likewise, if a circular peakon has nonzero angular momentum, then a full collapse to the origin will not occur. This result can be understood as follows. For a single rotating peakon, the Hamiltonian (39) becomes

$$H = \left(p^2 + \frac{M^2}{q^2}\right) G(q, q). \tag{48}$$

From the theory of Bessel functions we know that $G(q, q) \to \frac{1}{2}$ when $q \to 0$, and $G(q, q) > 0$ for all q. Moreover, it can be shown that

$$G(q, q) \geqslant \frac{1}{4(1 + q^2)}.$$

Thus, we have

$$H \geqslant \frac{M^2}{q^2} G(q, q) \geqslant \frac{M^2}{4q^2(1 + q^2)}.$$

Therefore, we conclude that $q^2(1+q^2) \geqslant M^2/(4H)$. Since q^2 is positive, we necessarily have $q \geqslant q_*(M, H) > 0$ with

$$q_*^2(M, H) = \frac{1}{2}\left(\sqrt{1 + \frac{M^2}{H}} - 1\right) \tag{49}$$

and so a peakon carrying angular momentum never collapses to the origin. This result can be formulated as the following proposition.

Proposition 6.1. *Consider a rotating radial peakon with given values of M, $H > 0$. In the process of its canonical evolution using Hamiltonian (48), this peakon cannot approach closer to the origin than $q_*(M, H)$ in equation (49).*

Remark. For $M \to 0$, $q_*(M, H) \sim M/\sqrt{4H} + O(M^3)$. Thus, for the same energy H, a circular peakon with smaller angular momentum, M, may approach closer to the origin.

7. Conclusions

The momentum map (16) for the action of diffeomorphisms on (closed) curves in the plane was used to generate invariant manifolds of singular solutions of EPDiff, the Euler–Poincaré equation (1) for geodesic motion on the diffeomorphism group. The H^1 norm of the fluid velocity was chosen for the kinetic energy of a class of solutions whose momentum support set was a family of N closed curves arranged as concentric circles on the plane. These finite-dimensional invariant manifolds of circularly symmetric solutions generalized the N-peakon (soliton) solutions of the Camassa–Holm equation from motion of points along the real line to motion in polar coordinates. This motion included rotation or, equivalently, circulation, which drives the radial motion. The momentum map with nonzero circulation for these concentric circles yielded a generalization of the circular CH peakons that included their rotational degrees of freedom. The canonical Hamiltonian parameters in the momentum map *and* solution ansatz (28) for the concentric rotating circular peakons provided a finite-dimensional Lagrangian description in polar coordinates of the flow governed by the Eulerian EP partial differential equation for geodesic motion (1). Numerically, we studied the basic interactions of these circular peakons amongst themselves, by collisions and by collapse to the centre, with and without rotation.

The main conclusions from our numerical study are the following.

- Momentum plays a key role in the dynamics. Radial momentum drives peakons to collapse into the centre, and azimuthal momentum prevents this collapse from occuring. Circular peakons were found to exhibit elastic collision behaviour (with its associated momentum and angular momentum exchanges, but with no excitation of any internal degrees of freedom) just as occurs in soliton dynamics. The same type of elastic collision behaviour has been verified to occur in the other, more geometrically complicated cases in [10].
- Collapse to the centre without rotation occurs with a bounded canonical momentum and with a vertical radial slope in velocity at $r = 0$, at the instant of collapse.
- For nonzero rotation, collapse to the centre cannot occur and the slope at $r = 0$ never becomes infinite.

The main questions that remain are the following.

- Numerical simulations show that a near-vertical or vertical slope occurs at head-on collision between two peakons of nearly equal height. A rigorous proof of this fact is still missing.
- It remains for us to discover whether a choice of Green's function exists for which the reduced motion is integrable on our $2N$-dimensional Hamiltonian manifold of concentric rotating circular peakons for $N > 1$.
- How does one determine the number and speeds of the rotating circular peakons that emerge from a given initial condition?
- How does the momentum map with internal degrees of freedom generalize to n dimensions?

All these challenging problems are beyond the scope of the present paper, and we will leave them as potential subjects for future work.

Acknowledgments

We are enormously grateful to our friends and colleagues for their scientific suggestions and help during the course of this work. We are especially grateful to Martin Staley for his help and cooperation in producing first class numerics for figure 1. We are also grateful for support and hospitality. DDH is grateful for support by US DOE, from contract W-7405-ENG-36 and from US DOE, Office of Science ASCAR/MICS. VP acknowledges the hospitality of the Los Alamos National Laboratory and Center for Nonlinear Studies, where he was able to spend one day a week during academic year 2002–2003. VP was partially supported by Petroleum Foundation Research Grant Number 40218-AC9. SNS acknowledges summer student support at the Theoretical Division at Los Alamos National Laboratory.

Appendix A. Extension of one-dimensional linear peakons to two dimensions

In this appendix, we show how to obtain the momentum line peakons, which are generalization of the line peakons. The standard ansatz for the regular one-dimensional peakon is

$$m(x,t) = \sum_{i=1}^{N} p_i(t)\delta(x - q_i(t)), \tag{50}$$

where m satisfies the one-dimensional version of equation (1). We propose the following extension of these solutions:

$$\boldsymbol{m}(x,t) = \sum_{i=1}^{N} (p_i(t)\hat{\boldsymbol{x}} + v_i(t)\hat{\boldsymbol{y}})\delta(x - q_i(t)), \tag{51}$$

where $\hat{\boldsymbol{x}}$, $\hat{\boldsymbol{y}}$ are unit vectors in the x, y directions, respectively. The solution lives on line filaments, which are parallel to the y-axis and propagate by translation along the x-axis. However, the y component of momentum now has a nontrivial value. Such solutions represent momentum lines that propagate perpendicular to the shock's front and 'slide' parallel to the front, moving surrounding 'fluid' with it. Upon substituting equation (51) into the equations of motion (1), we see that the x and y components of (1) both give the same equation of motion for $q_i(t)$:

$$\dot{q}_i(t) = \sum_j p_j G(q_i, q_j).$$

This compatibilty is what makes the factorized solution (51) possible. The equation of motion for p_i is

$$\dot{p}_i(t) = \sum_j (p_i p_j + v_i v_j) G'(q_i, q_j),$$

and for v_i,

$$\dot{v}_i = 0.$$

Thus, v_i can be considered as a set of parameters. (p_i, q_i) still satisfy Hamilton's canonical equations, with the Hamiltonian now given by

$$H = \frac{1}{2}\sum_{i,j=1}^{N} (p_i p_j + v_i v_j) G(q_i, q_j). \tag{52}$$

Finally, the 'angle' variables $y_i(t)$ conjugate to $v_i(t)$ with canonical Poisson bracket $\{y_i, v_j\} = \delta_{ij}$ satisfying

$$\dot{y}_i(t) = \sum_j v_j G(q_i, q_j).$$

Appendix B. Singular momentum solutions in cylindrical coordinates

The motion of N concentric circular rotating peakons in the plane may be extended into the third dimension, z, by envisioning a set of N circular rotating singular momentum 'rings' moving concentrically in various horizontal planes along a vertical cylindrical axis, as follows:

$$\boldsymbol{m}(r,z,t) = \sum_{a=1}^{N} \left(P^a(t)\hat{\boldsymbol{r}} + \frac{M^a(t)}{Q^a(t)}\hat{\boldsymbol{\phi}} + W^a(t)\hat{\boldsymbol{z}} \right) \frac{1}{r}\delta(r - Q^a(t))\delta(z - Z^a(t)). \tag{53}$$

By definition, the corresponding velocity is given by

$$\boldsymbol{u}(r,z,t) = \sum_i (G_i * m_i)\hat{\boldsymbol{\imath}} = \sum_{a=1}^{N} P^a(t) G_r(r, Q^a, z, Z^a)\hat{\boldsymbol{r}} + \frac{M^a(t)}{Q_r^a(t)} G_\phi \hat{\boldsymbol{\phi}} + W^a(t) G_z \hat{\boldsymbol{z}}. \tag{54}$$

The Green functions, G_i, for the three cylindrical components are found from the defining relations for the momentum in these coordinates,

$$
\begin{aligned}
m_r(r,z,t) &= \hat{\boldsymbol{r}}\cdot(\boldsymbol{u}-\Delta\boldsymbol{u}) &&= u_r - u_{r,rr} - \frac{1}{r}u_{r,r} + \frac{1}{r^2}u_r - u_{r,zz},\\
m_\phi(r,z,t) &= \hat{\boldsymbol{\phi}}\cdot(\boldsymbol{u}-\Delta\boldsymbol{u}) &&= u_\phi - u_{\phi,rr} - \frac{1}{r}u_{\phi,r} + \frac{1}{r^2}u_\phi - u_{\phi,zz},\\
m_z(r,z,t) &= \hat{\boldsymbol{z}}\cdot(\boldsymbol{u}-\Delta\boldsymbol{u}) &&= u_z - u_{z,rr} - \frac{1}{r}u_{z,r} - u_{z,zz}.
\end{aligned}
$$

Here the subscripts $,r$ and $,z$ denote differentiation with respect to r and z, and Δ is the Laplacian operator in cylindrical coordinates. The Green functions, G_i, are then

$$
\begin{aligned}
G_r(r,r',z,z') &= \frac{\mathrm{e}^{-k|z-z'|}}{2k\sqrt{1-k^2}}\begin{cases} I_1(\sqrt{1-k^2}r)K_1(\sqrt{1-k^2}r'), & r<r',\\ I_1(\sqrt{1-k^2}r')K_1(\sqrt{1-k^2}r), & r>r',\end{cases}\\
G_\phi(r,r',z,z') &= G_r(r,r',z,z'),\\
G_z(r,r',z,z') &= \frac{\mathrm{e}^{-k|z-z'|}}{2k\sqrt{1-k^2}}\begin{cases} I_0(\sqrt{1-k^2}r)K_0(\sqrt{1-k^2}r'), & r<r',\\ I_0(\sqrt{1-k^2}r')K_0(\sqrt{1-k^2}r), & r>r',\end{cases}
\end{aligned}
$$

where k is a constant that we may choose with the restriction $0<k<1$. (We have been using $\alpha=1$ for all of this. The constant k arises when solving for the Green functions using separation of variables.)

For solutions where $\boldsymbol{m}$ and $\boldsymbol{u}$ are functions of r, z, and t, but not ϕ, the equations of motion become

$$
\begin{aligned}
\frac{\partial m_r}{\partial t} &= -\frac{1}{r}\partial_r(rm_ru_r) - (rm_\phi)\partial_r\left(\frac{u_\phi}{r}\right) - \partial_z(m_ru_z),\\
\frac{\partial(rm_\phi)}{\partial t} &= -\frac{1}{r}\partial_r(r^2m_\phi u_r),\\
\frac{\partial m_z}{\partial t} &= -\frac{1}{r}\partial_r(rm_zu_r) - (rm_\phi)\partial_z\left(\frac{u_\phi}{r}\right) - \partial_z(m_zu_z).
\end{aligned}
$$

Written out explicitly, these equations are

$$
m_{r,t} = -2m_ru_{r,r} - u_rm_{r,r} - \frac{1}{r}m_ru_r - m_\phi u_{\phi,r} + \frac{1}{r}m_\phi u_\phi - u_zm_{r,z} - m_ru_{z,z} - m_zu_{z,r}, \quad (55)
$$

$$
m_{\phi,t} = -m_\phi u_{r,r} - u_rm_{\phi,r} - \frac{2}{r}m_\phi u_r - u_zm_{\phi,z} - m_\phi u_{z,z}, \quad (56)
$$

$$
m_{z,t} = -u_rm_{z,r} - m_zu_{r,r} - m_ru_{r,z} - \frac{1}{r}m_zu_r - m_\phi u_{\phi,z} - 2m_zu_{z,z} - u_zm_{z,z}. \quad (57)
$$

We shall obtain canonical equations of motion for the Lagrangian variables Q_i, P_i, M_i, Z_i, and W_i, where the solution ansatz for $\boldsymbol{m}$ and $\boldsymbol{u}$ given by (53) and (54) is inserted into the equations of motion (55)–(57). Upon integrating the resulting equations against an arbitrary smooth test function, $f(r,z)$, the following equations are obtained,

$$
\begin{aligned}
\dot{P}^a = -\sum_{b=1}^{N} & P^aP^b\partial_rG_r(Q^a,Q^b,Z^a,Z^b) + \frac{M^aM^b}{Q^aQ^b}\left(\partial_rG_\phi - \frac{G_\phi}{Q^a}\right)\\
&+W^aW^b\partial_rG_z(Q^a,Q^b,Z^a,Z^b),
\end{aligned} \quad (58)
$$

$$
\dot{Q}^a = \sum_{b=1}^{N} P^bG_r(Q^a,Q^b,Z^a,Z^b), \quad (59)
$$

$$\dot{Z}^a = \sum_{b=1}^{N} W^b G_z(Q^a, Q^b, Z^a, Z^b), \tag{60}$$

$$\partial_t \left(\frac{M}{Q^a} \right) = -\frac{M^a}{Q^a} \frac{1}{Q^a} \sum_{b=1}^{N} P^b G_r(Q^a, Q^b, Z^a, Z^b), \tag{61}$$

$$\dot{W}^a = -\sum_{b=1}^{N} P^a P^b \partial_z G_r + \frac{M^a M^b}{Q^a Q^b} \partial_z G_\phi + W^a W^b \partial_z G_z. \tag{62}$$

Relationships (58), (61) and 62) are obtained, from the r, ϕ and z components of momentum, respectively, by equating the terms $f(Q^a, Z^a)$. Equations (59) and (60) are obtained from each of the momentum equations by considering the terms containing $\partial_r f$ and $\partial_z f$, respectively. In fact, these considerations yield three copies of the evolution equations (59) and (60). Note that equation (61) simplifies to

$$\dot{M}^a = 0 \tag{63}$$

and so the M^a with $a = 1, \ldots, N$, provide N integrals of motion. With this in mind, we can see that the motion is Hamiltonian, with canonical variable pairs P^a, Q^a and Z^a, W^a. The corresponding Hamiltonian is

$$H = \frac{1}{2} \int \boldsymbol{m} \cdot \boldsymbol{u} = \frac{1}{2} \sum_{a,b=1}^{N} P^a P^b G_r + \frac{M^a M^b}{Q^a Q^b} G_\phi + W^a W^b G_z. \tag{64}$$

This Hamiltonian system has one additional conservation of motion, namely the total z-momentum; that is,

$$W = \sum_{a=1}^{N} W^a = \text{const}$$

is conserved.

References

[1] Arnold V I 1966 Sur la géométrie differentielle des groupes de Lie de dimenson infinie et ses applications à l'hydrodynamique des fluids parfaits *Ann. Inst. Fourier, Grenoble* **16** 319–61

[2] Camassa R and Holm D D 1993 An integrable shallow water equation with peaked solitons *Phys. Rev. Lett.* **71** 1661–4

[3] Camassa R, Holm D D and Levermore C D 1996 Long-time effects of bottom topography in shallow water *Physica* D **98** 258–86

[4] Kruse H P, Schreule J and Du W 2001 A two-dimensional version of the CH equation *Symmetry and Perturbation Theory: SPT 2001* ed D Bambusi *et al* (New York: World Scientific) pp 120–7

[5] Degasperis A, Holm D D and Hone A N W 2002 A new integrable equation with peakon solutions *Theor. Math. Phys.* **133** 1463–74

[6] Dullin H R, Gottwald G and Holm D D 2001 An integrable shallow water equation with linear and nonlinear dispersion *Phys. Rev. Lett.* **87** 194501–04

[7] Dullin H R, Gottwald G and Holm D D 2003 Camassa–Holm, Korteweg-de Vries-5 and other asymptotically equivalent equations for shallow water waves *Fluid Dyn. Res.* **33** 73–95

[8] Fringer O and Holm D D 2001 Integrable vs nonintegrable geodesic soliton behavior *Physica* D **150** 237–63

[9] Holm D D and Staley M F 2003 Wave structures and nonlinear balances in a family of evolutionary PDEs *SIAM J. Appl. Dyn. Syst.* **2** 323–80

[10] Holm D D and Staley M F Interaction dynamics of singular wave fronts *SIAM J. Appl. Dyn. Syst.* at press

[11] Holm D D and Marsden J E 2004 Momentum maps and measure-valued solutions (peakons, filaments and sheets) for the Euler–Poincaré equations for the diffeomorphism group *The Breadth of Symplectic and Poisson Geometry* ed J E Marsden and T S Ratiu (Boston, MA: Birkhäuser)

[12] Holm D D, Marsden J E and Ratiu T S 1998 The Euler–Poincaré equations and semidirect products with applications to continuum theories *Adv. Math.* **137** 1–81

[13] Miller M I and Younes L 2001 Group actions, homeomorphisms, and matching: a general framework *Int. J. Comput. Vision* **41** 61–84

[14] Holm D D, Rananather J T, Younes L and Trouvé A 2004 Soliton dynamics in computational anatomy *NeuroImage* at press

[15] Ortega J-P and Ratiu T S 2004 Momentum maps and Hamiltonian reduction *Progress in Mathamatics* vol 22 (Basle: Birkhaüser)

[16] Weinstein A 2002 Geometry of momentum *Preprint* math/SG0208108